The required area moment of inertia for the support rings is

$$I(\text{required}) = 9.31 \times 10^{-6} + 34.85 \times 10^{-6} = 44.16 \times 10^{-6}\ \text{m}^4\ (106.1\ \text{in.}^4)$$

This value is less than the value of $45.79 \times 10^{-6}\ \text{m}^4$ (110 in.^{4}) provided; therefore, the selected beam is satisfactory.

7.4. Suspension system design

One of the critical factors in the design of an effective cryogenic-fluid storage vessel is the method used to suspend the inner vessel within the outer vessel. A poor suspension system can nullify the effect of using a high-performance insulation. Some commonly used suspension systems are: (1) tension rods of high-strength stainless steel, (2) saddle bands of metal or plastic, (3) plastic (Micarta, for example) compression blocks, (4) multiple-contact supports (stacked discs), (5) compression tubes, and (6) wire cables or chains. A few of these systems are illustrated in Fig. 7.7.

The inner-vessel suspension system is subjected to the weight of the inner vessel and its contents plus dynamic loads that arise in transporting the vessel, earthquakes, and so on. Even if the storage vessel is a stationary vessel, it must withstand dynamic loads when empty during shipment if the vessel is not constructed on site. Seismic loads are possible for a vessel constructed on site. Some typical acceleration loadings that have

Fig. 7.7. Typical methods of supporting the inner vessel within the outer vessel in a dewar.

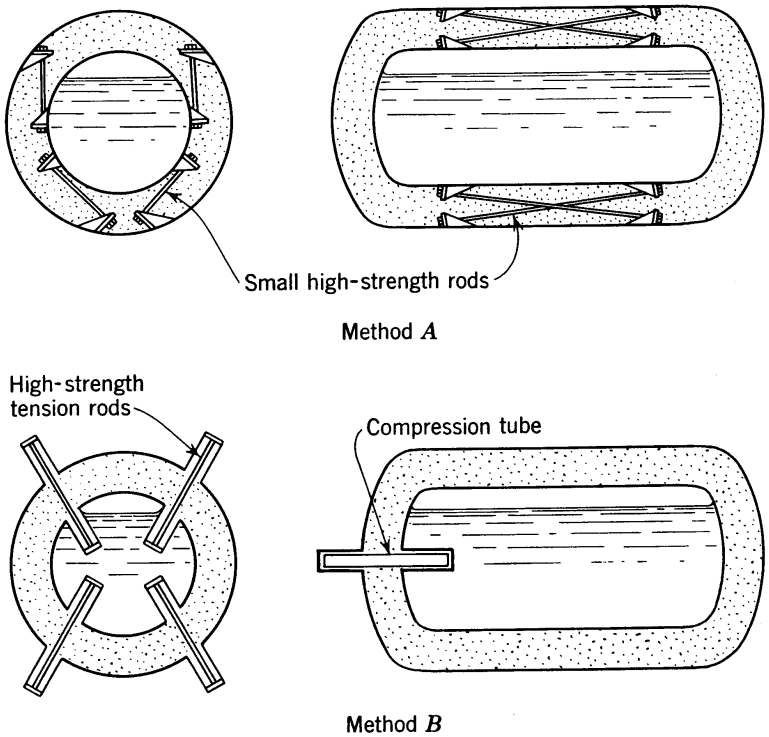

Table 7.7. Acceleration loads specified in suspension system design for cryogenic-fluid storage vessels

Type of unit	Vertical Up, g	Vertical Down, g	Transverse, g	Longitudinal g
Stationary storage vessels:				
Empty	0.5	3	0.5	5
Full	0.5	1.5	0.5	0.5
Full with blast loading	3	5	4	4
Transport trailers:				
Small (below 4 m^3 or 1060 gal U.S.)	2	5	4	8
Large (above 4 m^3)	1	4	2	4

been specified in design are given in Table 7.7. These loadings are given in multiples of the local acceleration due to gravity, so that a container subject to a 2-g acceleration load has a force equivalent to twice the container weight acting on the suspension system.

Let us analyze the suspension system loads for the case of high-strength tension rods, as shown in Fig. 7.7*a*. The suspension rods are arranged such that the rods support tensile loads only. The forces for vertical-down loading, vertical-up loading, and transverse loading (two cases) are shown in Fig. 7.8.

Fig. 7.8. Dynamic loading conditions for support system shown in Fig. 7.7*a*.

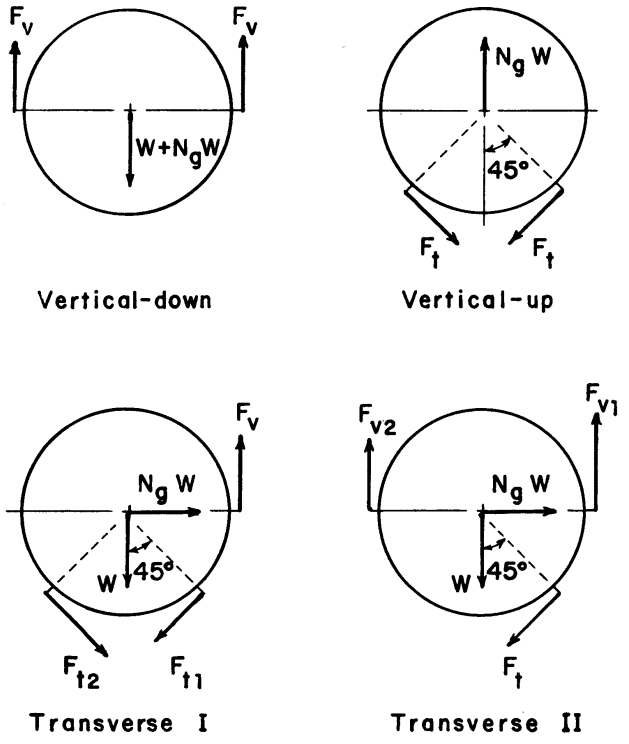

If we apply a force balance for the case of the vertical-down loading, we obtain

$$2F_v - W - N_g W = 0$$

Or, the force in one set of vertical rods is

$$F_v = (1 + N_g)W/2 \tag{7.17}$$

where N_g = acceleration load (Table 7.7)
W = weight of the inner vessel and its contents

By applying a similar force balance and moment balance (for the transverse loading), the forces in the suspension system can be obtained for the other cases. The results are summarized in Table 7.8.

If the angle between the longitudinal rods and the vessel wall is denoted by θ, then the acceleration load for the longitudinal rods is

$$F_l = N_g W/\cos\theta \tag{7.18}$$

Two sets of longitudinal rods must be used—one set for forward loading and another set for rearward loading.

For safety reasons, generally two or more rods are used at each support point. The support rods are attached at the main support rings on the outer vessel and at one of the inner-vessel stiffening rings. Resistance to heat transfer down the rods may be achieved by using springs or washers at either end or both ends of the support members. Spherical washers may be used to reduce misalignment of the rods resulting from thermal contraction of the inner vessel. A typical support bracket is shown in Fig. 7.9.

The heat-transfer rate down a support rod may be determined from the

Table 7.8. Forces in the vertical and transverse rods for the cases shown in Fig. 7.8

Loading	Force in Rods
Vertical-down	$F_v = (1 + N_g)W/2$
Vertical-up	$F_t = N_g W/\sqrt{2}$
Transverse (I)	For $(\sqrt{2} - 1)N_g \geqq 1$ or $N_g \geqq 2.414$
	$F_v = \sqrt{2}\, N_g W$
	$F_{t1} = [(\sqrt{2} + 1)N_g - 1]W/\sqrt{2}$
	$F_{t2} = [(\sqrt{2} - 1)N_g - 1]W/\sqrt{2}$
Transverse (II)	For $N_g < 2.414$
	$F_{v1} = [1 + (\sqrt{2} + 1)N_g]W/2$
	$F_{v2} = [1 - (\sqrt{2} - 1)N_g]W/2$
	$F_t = \sqrt{2}\, N_g W$

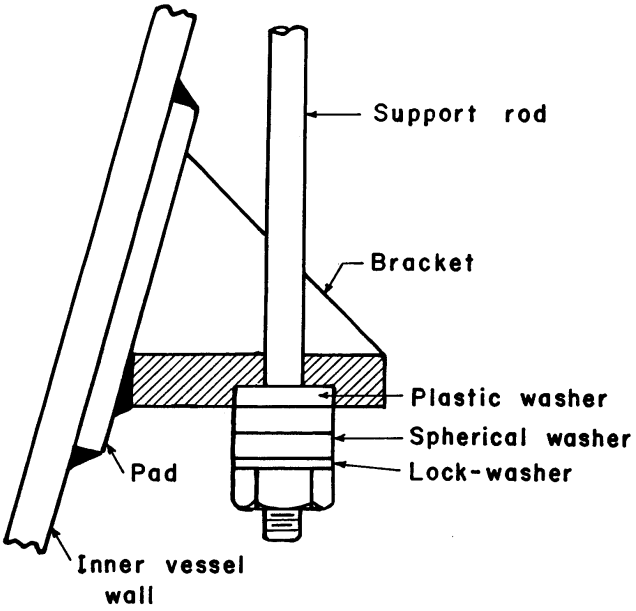

Fig. 7.9. Typical support bracket detail for suspension systems of dewars.

Fourier rate equation considering the effect of variable thermal conductivity:

$$\dot{Q} = \frac{k_m A(T_h - T_c)}{L} = (K_h - K_c)\left(\frac{A}{L}\right) \tag{7.19}$$

where k_m = mean thermal conductivity of rod = $(K_h - K_c)/(T_h - T_c)$
T_h = temperature of the warm end of the rod
T_c = temperature of the cold end of the rod
A = cross-sectional area of the rod
L = length of the rod
$K = \int_{4K}^{T} k_t \, dT$ = thermal conductivity integral

Values for the thermal conductivity integral are given in Table 7.9 for several materials.

Example 7.3. Design the support system for the liquid-oxygen storage container in Example 7.1, if the support system consists of 20-mm diameter (0.787-in.) stainless-steel rods with an allowable stress of 500 MPa (72,500 psi). The vessel is a stationary vessel, and the design acceleration loads are given in Table 7.7. The angle between the longitudinal rods and the vessel wall is $\theta = 9°$.

From Example 7.1, we found the total vessel weight to be 1310 kN when full

Table 7.9. Thermal conductivity (k_t, W/m-K) and thermal conductivity integral (K, W/m) for selected materials (Stewart and Johnson 1961) $K = \int_{4K}^{T} k_t\, dT$

Temperature	Beryllium Copper		Aluminum (6063-T5)		Low-Carbon Steel (C1020)		Stainless Steel (304)		Monel (drawn)		Teflon	
(K)	k_t	K	k_t	K	k_t	K	k_t	K	k_t	K	k_t	K
4	1.9	0	34	0	3.0	0	0.24	0	0.43	0	0.046	0.0
10	4.8	19	86	360	11.5	43	0.77	2.9	1.74	6.3	0.096	0.44
20	10.6	95	170	1,650	24.0	222	1.95	16.3	4.30	36.4	0.141	1.64
30	16.2	229	230	3,650	32.0	502	3.30	42.4	6.90	92.9	0.174	3.23
40	21.0	415	270	6,200	38.6	867	4.70	82.4	9.00	173	0.193	5.08
50	26.1	650	280	8,950	47.6	1,310	5.80	135	10.95	273	0.208	7.16
60	30.0	930	270	11,700	53.6	1,810	6.80	198	12.09	368	0.219	9.36
70	33.7	1,250	248	14,300	57.5	2,360	7.60	270	13.06	513	0.228	11.6
80	37.0	1,600	230	16,700	60.0	2,950	8.26	349	13.90	647	0.235	13.9
90	40.1	1,990	222	19,000	61.8	3,550	8.86	436	14.63	791	0.241	16.3
100	43.0	2,400	216	21,100	62.9	4,170	9.40	528	15.27	940	0.245	18.7
120	48.4	3,300	207	25,300	64.1	5,450	10.36	726	16.26	1,260	0.251	23.7
140	53.3	4,320	201	29,300	64.6	6,750	11.17	939	17.34	1,590	0.255	28.7
160	57.6	5,440	200	33,300	64.8	8,050	11.86	1,170	18.25	1,950	0.257	33.8
180	61.5	6,640	200	37,300	64.9	9,350	12.47	1,410	19.02	2,320	0.258	39.0
200	65.0	7,910	200	41,300	65.0	10,700	13.00	1,660	19.69	2,710	0.259	44.2
250	72.4	11,300	200	51,300	65.0	13,900	14.07	2,340	21.02	3,730	0.260	57.2
300	78.5	15,000	200	61,300	65.0	17,200	14.90	3,060	22.00	4,800	0.260	70.2

and 124 kN when empty. For the full vessel, we find the following forces in the support rods:

1. Vertical-down loading, $N_g = 0.5$.

$$F_v = (1 + 0.5)(1310)/(2) = 982.5 \text{ kN (vertical rods)}$$

2. Vertical-up loading, $N_g = 1.5$.

$$F_t = (1.5)(1310)/\sqrt{2} = 1389.5 \text{ kN (transverse rods)}$$

3. Transverse loading, $N_g = 0.5 < 2.414$ (Case II applies).

$$F_{v_1} = [1 + (\sqrt{2} + 1)(0.5)](1310)/(2) = 1445.7 \text{ kN (vertical rods)}$$
$$F_{v_2} = [1 - (\sqrt{2} - 1)(0.5)](1310)/(2) = 519.3 \text{ kN}$$
$$F_t = (\sqrt{2})(0.5)(1310) = 926.3 \text{ kN}$$

If we repeat the calculations of the empty-vessel case ($W = 124$ kN), we obtain the following support-rod forces:

1. Vertical-down loading, $N_g = 0.5$, $F_v = 93.0$ kN.
2. Vertical-up loading, $N_g = 3$, $F_t = 263.0$ kN.
3. Transverse loading, $N_g = 0.5$.

$$F_{v_1} = 136.8 \text{ kN}, \qquad F_{v_2} = 49.2 \text{ kN}, \qquad F_t = 87.7 \text{ kN}$$

From these calculations, we find that the largest loadings are

F_t = 1389.5 kN (312,360 lb_f), for vertical-up loading, full vessel
F_v = 1445.7 kN (324,990 lb_f) for transverse loading, full vessel

For the full vessel, the force in the longitudinal rods in one direction ($N_g = 0.5$) is

$$F_l = (0.5)(1310)/\cos 9° = 663.2 \text{ kN (full vessel)}$$

For the empty vessel ($N_g = 5$), we find $F_l = 627.7$ kN, so the full-vessel case results in the larger load.

The design force in one rod is

$$F_d = s_a A = (500)(10^3)(\tfrac{1}{4}\pi)(0.020)^2 = 157.08 \text{ kN}$$

The required number of rods for one side of the vessel is as follows:

$$N_v = F_v/F_d = 1445.7/157.08 = 9.2 \text{ rods}$$

Because there are two support points on each side of the vessel (front and back), the number of rods must be an even number. Therefore, we will select

$$N_v = 10 \text{ rods on each side}$$

or 5 rods at each of the four support points in the vertical direction. Similarly, the number of transverse rods is

$$N_t = F_t/F_d = 1389.5/157.08 = 8.8 \text{ rods}$$

We will select

$$N_t = 10 \text{ rods on each side}$$

or 5 rods at each of the four support points in the transverse direction. For the longitudinal rods,

$$N_l = F_l/F_d = 663.2/157.08 = 4.2 \text{ rods}$$

We will select

$$N_l = 6 \text{ rods in each direction}$$

or 12 rods total (both directions).

7.5. Piping

Piping necessary to remove liquid from the container, vent vapor from the vessel, and so on, introduces a source of heat inleak to the product container. With a properly designed piping system, the heat transfer down the piping is due to conduction along the pipe wall only. For this reason, the piping runs should be made as long as possible, and thin-walled pipe should be used. Schedule 5 pipe (the thinnest piping available in 304 stainless steel) or schedule 10 pipe is typically used in many larger cryogenic-fluid storage vessels. The thermal contraction of the piping runs must be considered in the piping system design also.

(between 40 and 50 percent by weight), the thermal conductivity of an evacuated powder can be reduced by a factor of 5. Some values of thermal conductivity for opacified powder insulations are given in Table 7.16.

From a safety standpoint, copper flakes were found to be preferable to aluminum because aluminum has a large heat of combustion in combination with oxygen. If an aluminum opacified powder were used to insulate a liquid-oxygen container, there would be a constant hazard from any leaks of oxygen into the vacuum space. Copper opacified powders have been used with complete safety.

Opacified powders have the disadvantage that vibration can cause packing of the metal flakes. If many flakes get packed together, a "thermal short" develops, and the thermal conductivity of the insulation is increased.

7.13. Multilayer insulations

Multilayer insulations consist of alternating layers of a highly reflecting material, such as aluminum foil, copper foil, or aluminized Mylar, and a low-conductivity spacer, such as fiberglass mat or paper, glass fabric, or nylon net. The reflecting layers may also be separated by crinkling or embossing the sheets so that they touch only at a few discrete points, and a spacer is not required.

This insulation was first developed by P. Peterson of Sweden in 1951 (Peterson 1958). Since that time several investigators have studied various types of multilayer insulation and application techniques for improving the insulation performance (Kropschot et al. 1960; Hnilicka 1960; Black and Glaser 1961; Matsch 1962; Caren and Cunningham 1968).

Multilayer insulations must be evacuated to pressures below 10 mPa (7.5×10^{-5} torr) to be effective. The dependence to the apparent thermal conductivity on residual gas pressure for a typical multilayer insulation is shown in Fig. 7.15. Representative thermal conductivity values are presented in Table 7.17.

Table 7.16. Thermal conductivity of opacified powder insulations. The boundary temperatures are 300 K (80°F) and 77.4 K (−321°F), and the residual gas pressure is below 0.13 Pa (0.001 torr).

Insulation	Density		Thermal Conductivity	
	kg/m³	lb_m/ft^3	mW/m-K	Btu/hr-ft-°F
50/50 w/w Copper-Santocel	180	11.2	0.33	0.19×10^{-3}
40/60 w/w Aluminum-Santocel	160	10.0	0.35	0.20×10^{-3}
50/50 w/w Bronze-Santocel	179	11.2	0.58	0.33×10^{-3}
Silca-carbon	80	5.0	0.48	0.28×10^{-3}

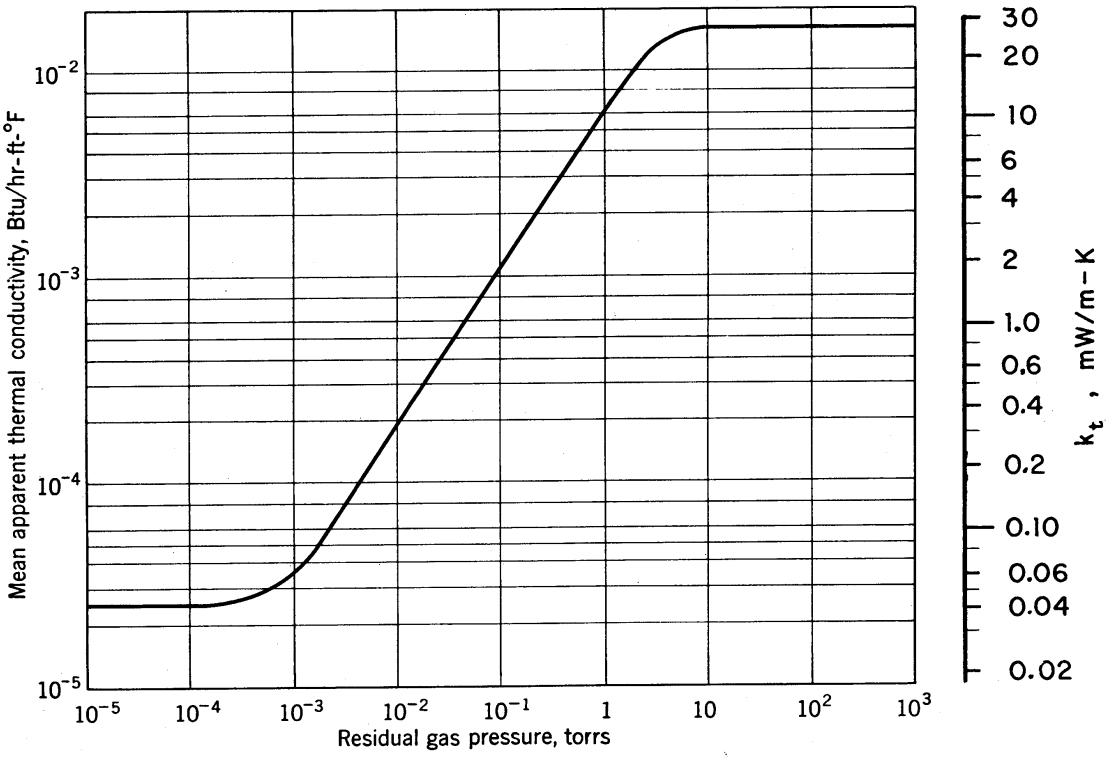

Fig. 7.15. Variation of mean apparent thermal conductivity with residual gas pressure for a typical multilayer insulation. The insulation layer-density is 24 layers/cm (60 layers/in.), and the boundary temperatures are 300 K (540°R) and 90.5 K (163°R).

Table 7.17. Thermal conductivity for multilayer insulations for boundary temperatures of 300 K (80°F) and 77.4 K (−321°F) with residual gas pressures of 1.3 mPa (10^{-5} torr)

Insulation	Layer Density		Thermal Conductivity	
	layer/cm	layer/in.	μW/m-K	Btu/hr-ft-°F
0.006-mm aluminum foil + 0.15-mm Fiberglass paper	20	50	37	2.1×10^{-5}
0.006-mm aluminum foil + 2-mm mesh rayon net	10	25	78	4.5×10^{-5}
0.006-mm aluminum foil + 2-mm mesh nylon net	11	28	34	2.0×10^{-5}
NRC-2 crinkled aluminized Mylar film 0.006 mm	35	89	42	2.4×10^{-5}
Dimplar dimpled + smooth Mylar film	8	20	42	2.4×10^{-5}
0.0087-mm aluminum foil + carbon-loaded glass-fiber paper[a]	30	76	14	0.85×10^{-5}

[a]Residual gas pressure = 0.4 mPa = 3×10^{-6} torr

The amazingly low thermal conductivity of multilayer insulations can be explained by the fact that all modes of heat transfer—radiation, solid conduction, and gaseous conduction—are reduced to a bare minimum. Radiation is minimized by using many layers of a highly reflecting metal foil. Solid conduction through the spacer material is minimized by using a low-conductivity fiberous material or by crinkling the shield material to allow contact at only a few points. Gaseous conduction is minimized by reducing the residual gas pressure to values on the order of 1.3 mPa (10^{-5} torr).

The bulk density of multilayer insulations depends upon the thickness and density of the reflective shields, the type of spacer material used, and the layer density or number of layers per unit thickness:

$$\rho_a = (S_s + \rho_r t_r)(N/\Delta x) \tag{7.39}$$

where S_s is the mass of spacer material per unit area, ρ_r is the density of the shield material, t_r is the thickness of the radiation shields, and $N/\Delta x$ is the layer density (one layer is defined as one sheet of foil plus one sheet of spacer material). Typical densities of multilayer insulations range between 32 kg/m^3 to 320 kg/m^3 (2 to 20 lb$_m$/ft^3), with layer densities ranging from 8 layers/cm to 40 layers/cm (20 to 100 layers/in.).

For a well-evacuated multilayer insulation, heat is transmitted primarily by radiation and solid conduction through the spacer material. For this situation, the apparent thermal conductivity may be determined from

$$k_t = (N/\Delta x)^{-1}[h_c + \sigma e(T_h^2 + T_c^2)(T_h + T_c)/(2 - e)] \tag{7.40}$$

where h_c is the solid conductance for the spacer material, σ is the Stefan-Boltzmann constant, e is the effective emissivity of the shield material, and T_h and T_c are the boundary temperatures of the insulation. From eqn. (7.40) we see that the apparent thermal conductivity of a multilayer insulation can be reduced by increasing the layer density up to a certain point. If the insulation is compressed too tightly, the solid conductance increases faster than $N/\Delta x$, so the insulation conductivity also increases. The variation of the apparent thermal conductivity with layer density for a typical multilayer insulation is shown in Fig. 7.16.

The thermal conductivity of multilayer insulations in the direction parallel to the shields is about three orders of magnitude greater than the thermal conductivity in the direction normal to the shields (Vliet and Coston 1968). Because of this characteristic, care must be exercised in applying the multilayer insulation around penetrations through the insulation. The insulation performance will be seriously degraded if the edges of the shields are allowed to contact the vent line, for example.

One of the problems associated with the use of multilayer insulations is the effective evacuation of the residual gas from the space within the

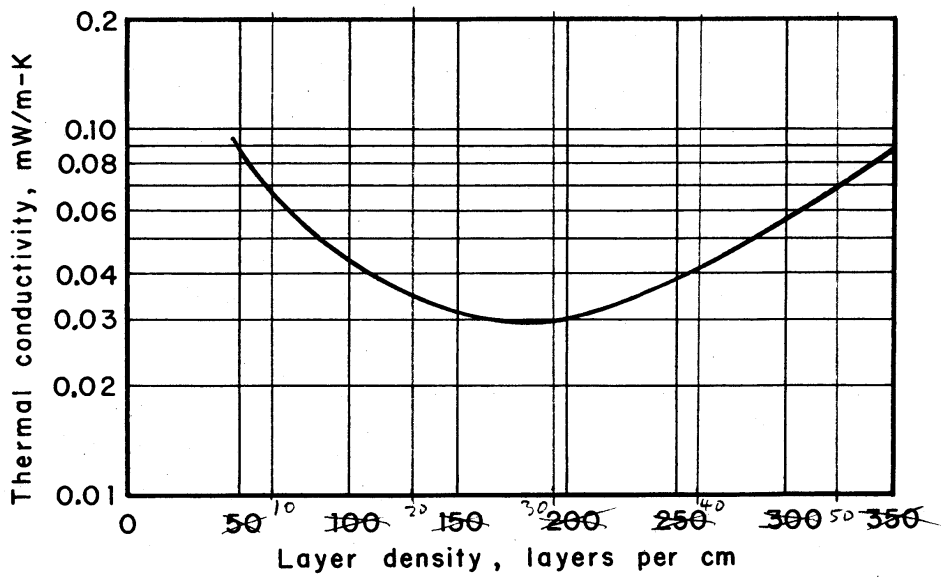

Fig. 7.16. Variation of thermal conductivity with layer density for a typical multilayer insulation (Wang 1961). The boundary temperatures are 294 K (530°R) and 78 K (140°R).

insulation layer. Small vent holes have been used in the foil layers to allow more effective removal of the trapped gas. Scurlock and Saull (1976) have shown that outgassing of the shields can also introduce significant quantities of gas within the insulation. They developed a multilayer insulation using carbon-filled glass-fiber paper for the spacer material. The carbon acted as a getter to absorb the outgassing load and maintain a low pressure within the insulation. The resulting multilayer insulation had an apparent thermal conductivity of 14 μW/m-K (8.5×10^{-6} Btu/hr-ft-°R), as shown in Table 7.17.

7.14. Comparison of insulations

A comparison of the advantages and disadvantages of the insulations used in cryogenic systems is given in the following summary.

Advantages	Disadvantages
1. *Expanded foams*	
Low cost.	High thermal contraction.
No need for rigid vacuum jacket.	Conductivity may change with time.
Good mechanical strength.	
2. *Gas-filled powders and fiberous materials*	
Low cost.	Vapor barrier is required.
Easily applied to irregular shapes.	Powder can pack and conductivity is increased.
Not flammable.	

Advantages	Disadvantages
3. *Vacuum alone*	
Complicated shapes may be easily insulated.	A permanent high vacuum is required.
Small cool-down loss.	Low-emissivity boundary surfaces needed.
Low heat flux for small thickness between inner and outer vessel.	
4. *Evacuated powders and fibrous materials*	
Vacuum level less stringent than for multilayer insulations.	May pack under vibratory loads and thermal cycling.
Complicated shapes may be easily insulated.	Vacuum filters are required. Must be protected when exposed to moist air (retains moisture).
Relatively easy to evacuate.	
5. *Opacified powders*	
Better performance than straight evacuated powders.	Higher cost than evacuated powders.
Complicated shapes may be easily insulated.	Explosion hazards with aluminum in an oxygen atmosphere.
Vacuum requirement is not as stringent as for multilayer insulations and vacuum alone.	Problems of settling of metallic flakes.
6. *Multilayer insulations*	
Best performance of all insulations.	High cost per unit volume.
Low weight.	Difficult to apply to complicated shapes.
Lower cool-down loss compared with powders.	Problems with lateral conduction.
Better stability than powders.	More stringent vacuum requirements than powders.

7.15. Vapor-shielded vessels

Another method of reducing the heat inleak to a cryogenic-fluid storage vessel is to use the cold vent gas to refrigerate an intermediate shield, as shown in Fig. 7.17. The escaping vent gas intercepts some of the heat that would otherwise find its way to the product liquid. The effectiveness of this method in reducing the heat inleak depends upon the ratio of sensible heat absorbed by the vent gas to the latent heat of the fluid, as indicated in the following analysis.

The heat-transfer rate from ambient to the vapor shield through all paths may be written

$$\dot{Q}_{2-s} = U_2(T_2 - T_s) = U_2[(T_2 - T_1) - (T_s - T_1)] \tag{7.41}$$

where the coefficient U_2 may be determined from

$$U_2 = (k_t A/\Delta x)_{\text{ins}} + (k_t A/\Delta x)_{\text{sup}} + (k_t A/\Delta x)_{\text{piping}} \tag{7.42}$$

where k_t is the thermal conductivity for the insulation, supports, or piping; A is the heat-transfer area for each of these components; and Δx is the length of conduction path (thickness for the insulation, support length for vessel supports, and piping length for piping). The heat-transfer rate